JOURNAL OF GEOPHYSICAL RESEARCH, VOL. 106, NO. D6, PAGES 5151–5160, MARCH 27, 2001

Subpixel canopy cover estimation of coniferous forests in Oregon using SWIR imaging spectrometry

David B. Lobell and Gregory P. Asner

Department of Geological Sciences and Environmental Studies Program, University of Colorado, Boulder, Colorado

Beverly E. Law

College of Forestry, Oregon State University, Corvallis, Oregon

Robert N. Treuhaft

Jet Propulsion Laboratory, California Institute of Technology, Pasadena, California

Abstract. The percent cover of vegetation canopies is an important variable for many land-surface biophysical and biogeochemical models and serves as a useful measure of land cover change. Remote sensing methods to estimate the subpixel fraction of vegetation canopies with spectral mixture analysis (SMA) require knowledge of the reflectance properties of major land cover units, called endmembers. However, variability in endmember reflectance across space and time has limited the interpretation and general applicability of SMA approaches. In this study, a subpixel vegetation cover of coniferous forests in Oregon, United States, was successfully estimated by employing shortwave infrared reflectance measurements (SWIR2 region, 2080–2280 nm) collected by the NASA Airborne Visible Infrared Imaging Spectrometer (AVIRIS). The approach presented here, referred to as AutoSWIR [*Asner and Lobell*, 2000], was originally developed for semiarid and arid environments and exploits the low SWIR2 variability of materials found in most ecosystems. SWIR2 field spectra from Oregon were compared with spectra from an arid systems database, revealing significant differences only for soil reflectance. However, SWIR2 variability remained low, as indicated by field spectra and principal component analysis, and AutoSWIR was then modified to use coniferous forest spectra collected in Oregon. Subsequent high spatial resolution estimates of forest canopy cover agreed well with estimates from low-altitude air photos (rms = 3%), demonstrating the successful extension of AutoSWIR to a coniferous forest ecosystem. The generality of AutoSWIR facilitates accurate estimates of vegetation cover that can be automatically retrieved from SWIR2 spectral measurements collected by forthcoming spaceborne imaging spectrometers such as NASA's New Millenium Program EO-1 Hyperion. These estimates can then be used to characterize landscape heterogeneity important for land-surface, atmospheric, and biogeochemical research.

1. Introduction

Spatial heterogeneity of forest canopy cover plays a major role in determining the flux of energy and materials between the land surface and the atmosphere [e.g., *Sellers et al.*, 1997; *Pielke et al.*, 1998]. It also affects the habitability and biological diversity of ecosystems [*Denslow*, 1995]. Canopy cover is an important parameter in a variety of land-surface biophysical and biogeochemical models sensitive to landscape heterogeneity [e.g., *Running et al.*, 1994; *Bonan*, 1995]. Numerous studies have demonstrated the strong effect of surface heterogeneity on factors such as hydrology [*Ghan et al.*, 1997], roughness length [*Oleson et al.*, 2000], and albedo [*Rowe*, 1993] which are important for land-atmosphere interactions. For example, *Yang et al.* [1999] showed that the areal coverage of vegetation strongly affects ground heat flux calculations critical to atmospheric models. In addition, canopy cover is widely used in analyses of carbon storage deemed important for management and policy development [*Houghton et al.*, 1993].

Several studies have indicated that coniferous forests in temperate and boreal biomes are especially important in the global carbon cycle, since they currently contain 16–24% of the world's soil carbon [*Gates*, 1993] and are susceptible to global warming [e.g., *Sellers et al.*, 1996]. However, unresolved heterogeneity in vegetation properties in these ecosystems can be significant; *Kimball et al.* [1999], for instance, found that subpixel-scale land cover complexity in boreal forests could lead to annual net primary production (NPP) errors of more than 14% using an ecosystem process model. In another study, *Bonan et al.* [1993] showed that landscape heterogeneity in coniferous forests had a highly nonlinear effect on sensible heat and evapotranspiration calculations, with errors as high as 46% and 15%, respectively. The ability to accurately estimate vegetation cover in coniferous forests, and thereby constrain models used to understand land-surface, atmospheric, and biogeochemical processes, is of great importance in these regions. Remote sensing is a relatively cheap and fast method for estimating

Paper number 2000JD900739.
0148-0227/01/2000JD900739$09.00

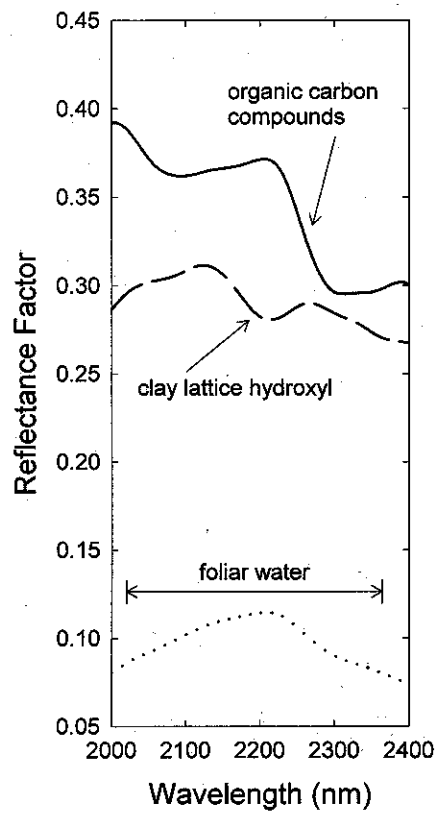

Figure 1. Typical spectra of green canopy (dotted), litter (solid), and bare soil (dashed) in SWIR2 region (2000–2400 nm). Primary causes of major spectral features are provided.

forest canopy cover across broad geographic regions, but previous studies show that functionally important cover variation can occur at very high spatial resolution, such as within image pixels of just tens of square meters in size [e.g., *Spanner et al.*, 1990; *Cohen et al.*, 1990; *Hall et al.*, 1995]. This presents a problem to studies focused on processes sensitive to forest gap fraction, stand density, and intercanopy spacing.

Spectral mixture analysis (SMA) has proven useful for estimating image subpixel land cover fractions from remotely sensed data [e.g., *Roberts et al.*, 1993; *Smith et al.*, 1994; *Bateson and Curtis*, 1996]. Two major assumptions of traditional SMA approaches are as follows: (1) The total pixel reflectance is a linear combination of the endmember reflectance; (2) the reflectance of each endmember does not vary across an image. While the first assumption has proven reasonable in many ecosystems at the landscape scale [*Wessman et al.*, 1997; *Villenueve et al.*, 1998], variability of endmember reflectance is a major obstacle to accurately using SMA approaches [*Price*, 1994; *Roberts et al.*, 1998; *Bateson et al.*, 2000]. Endmember variability can result from many factors, including changes in vegetation species, architecture, and/or condition, soil properties, and shading effects [e.g., *Ross*, 1981; *Myneni et al.*, 1989; *Jacquemoud et al.*, 1992; *Pinty et al.*, 1998]. Ultimately, this variability impedes regional-scale analyses of vegetation cover and associated processes such as disturbance response, both of which are considered to be crucial in land-surface and atmosphere analyses [*Sellers et al.*, 1997].

In a study of arid and semiarid regions, *Asner et al.* [2000] and *Asner and Lobell* [2000] showed that the reflectance variability of major land cover types (e.g., green vegetation, senescent vegetation, and soil) was dominated by variation in overall albedo of the shortwave region from 400 to 2500 nm. They also showed that the shape (or derivative) of the reflectance spectra in the shortwave-infrared region (SWIR2) from 2080 to 2280 nm was consistent and distinct between land cover types (Figure 1). By normalizing the SWIR2 reflectance spectra to 2080 nm, the variability within green vegetation, litter, and soil endmember classes was significantly reduced, while the endmember classes themselves were distinct from one another. This enabled the development of an automated spectral unmixing method for determining the fractional (image subpixel) cover of green vegetation, soils, and senescent vegetation (litter) from SWIR2 hyperspectral reflectance measurements collected by NASA's Airborne Visible-Infrared Imaging Spectrometer (AVIRIS).

While this model AutoSWIR [*Asner and Lobell*, 2000] was developed for arid and semiarid shrublands and grasslands, the biogeophysical properties of the cover types that give rise to the method were general and could potentially work in many other ecosystem types. For example, the consistent shapes of green and senescent vegetation spectra in the SWIR2 are due to strong foliar water and organic compound absorptions, respectively [*Gates et al.*, 1965; *Woolley*, 1971; *Curran*, 1989], which are general properties of vegetation (Figure 1). On the other hand, the characteristic absorption feature of soils at ~2200 nm is due to the clay lattice hydroxyl and can change both in magnitude and in position depending on the specific mineral composition [*Irons et al.*, 1989; *Ben-Dor et al.*, 1999]. In an effort to generalize the AutoSWIR approach to new ecosystems, it is important to understand the potential variability of endmember spectra from other environments and to develop the best approach by which this variability can be accommodated.

The goal of this study was to determine the accuracy of the AutoSWIR algorithm applied to data collected by the AVIRIS over temperate coniferous forests of central Oregon. In particular, we sought to (1) evaluate the effectiveness of using the original arid land spectra [from *Asner and Lobell*, 2000] in AutoSWIR, (2) assess differences in algorithm performance when using spectra collected at field sites in Oregon, and (3) explore the potential of a three-band SWIR2 index, first introduced by *Asner and Lobell* [2000], for operational subpixel cover estimation using multispectral imaging technologies.

2. Methods

2.1. Site Description

We conducted the study on the east side of the Cascade Mountains in central Oregon, where there is a strong climatic gradient and forest transition from Douglas fir (*Pseudotsuga menziesii*) and grand fir (*Abies grandis*) to the dry eastern extent of Ponderosa pine (*Pinus ponderosa* var. Laws). The climate of the *P. ponderosa* zone is semiarid (annual rainfall, 350–760 mm), with minimal summer precipitation. The overall study region was ~576 km^2. Within this region we located twenty 100 × 100 m plots along an east-west swath that includes *P. menziesii*, *A. grandis*, larch (*Larix occidentalis*), cedar (*Calocedrus decurrens*), and *P. ponderosa* forests (Table 1). About 75% of the plots are totally *P. ponderosa* or mixes with *P. menziesii*, *A. grandis*, or *C. decurrens*. A few of the pine sites were less productive, existing on a perched water table on a clay layer closer to the surface. We selected plots to encompass

Table 1. Summary of Vegetation and Soil Variation Across the Study Plots Used to Evaluate the AutoSWIR Algorithm[a]

Plot	Easting, m	Northing, m	Altitude, m	Dominant Species	Soil Class	Canopy Cover, %
1	609333	4927976	909.7	Pipo	ALFIC VITRIXERANDS	61
2	609494	4928171	905.4	Pipo	ALFIC VITRIXERANDS	48
3	609495	4927935	912.5	Pipo	ALFIC VITRIXERANDS	70
4	608907	4922658	934.8	Pipo	ALFIC VITRIXERANDS	68
5	607268	4920812	916.8	Pipo	ALFIC VITRIXERANDS	62
6	605981	4922809	918.0	Pipo	AQUIC VITRIXERANDS	68
7	606203	4922938	914.7	Pipo	ALFIC VITRIXERANDS	73
8	606270	4923123	911.5	Laoc	ALFIC VITRIXERANDS	73
9	604497	4922255	935.2	Pipo	UMBRIC VITRIXERANDS	...
10	612709	4920153	1147.0	Pipo	ALFIC VITRIXERANDS	59
11	614861	4922815	1250.0	Pipo	XERIC VITRICRYANDS	63
12	602613	4920950	986.9	Abgr	TYPIC VITRICRYANDS	70
13	604321	4922333	936.4	Laoc	UMBRIC VITRIXERANDS	...
14	603110	4919591	996.6	Abgr	UMBRIC VITRIXERANDS	76
15	606517	4920410	924.1	Pipo	HUMIC VITRIXERANDS	56
16	605918	4920714	922.1	Pipo	UMBRIC VITRIXERANDS	85
17	606418	4924017	909.1	Pipo	ALFIC VITRIXERANDS	76
18	610761	4920518	1132.0	Cade	ALFIC VITRIXERANDS	...
19	607370	4920296	916.9	Pipo	ALFIC VITRIXERANDS	69
20	614056	4921252	1185.0	Pipo	ULTIC HAPLOXERALFS	...

Species codes: Pipo, *Pinus ponderosa*; Laoc, *Larix occidentalis*; Cade, *Calocedrus decurrens*; Psme, *Pseudotsuga menziessii*; Abgr, *Abies grandis*.
[a]Also shown are the green canopy cover estimates from low-altitude aerial photography (available at 16 plots).

a range of stand densities (trees/area). Two of the plots were primarily *A. grandis/P. menziesii*, two were *L. occidentalis* (one of which had been heavily logged and only had a few trees on it), and one was dominated by *C. decurrens*. The pine sites included young regenerating forests (<10 m tall), mature, and old-growth forests. The plots were also selected to span the full range of soil substrates in the study area, from a gravely loam surface in the *A. grandis/P. menziesii* forests closer to the mountains, to sandy pumice soils in *P. ponderosa* forests (Table 1).

2.2. AVIRIS Data

The NASA Airborne Visible and Infrared Imaging Spectrometer (AVIRIS) collects upwelling radiance data in 224 optical channels with a nominal full width at half maximum (FWHM) of 10 nm covering a spectral range of 380–2500 nm [*Green et al.*, 1998]. The AVIRIS was flown over the study region on June 10, 1999, on the NASA ER-2 aircraft at 20 km altitude, creating ~17 × 17 m pixels in the resulting image data. Radiance data were converted to apparent surface reflectance using the ATREM atmospheric code [*Gao et al.*, 1993], which employs the 6S scattering code for atmospheric gases [*Vermote et al.*, 1996]. Further corrections for SWIR2 reflectance were made using a large (dark) lake and (bright) cumulus clouds. Assuming both targets to be spectrally flat in the SWIR2 (*Gao and Goetz* [1990] and our field spectra from lake), the ATREM-corrected reflectance values were used to create a gain and offset for each SWIR2 band, which were then applied to complete the reflectance calibration. This final step was necessary to remove apparent errors in the ATREM correction for methane, which strongly absorbs radiation beginning at ~2200 nm.

2.3. Spectral Mixture Model

The AVIRIS reflectance data were processed to fractional abundance images with the AutoSWIR algorithm (Figure 2) [*Asner and Lobell*, 2000]. A field spectral database of green canopies, litter canopies, and soils was high-frequency filtered to remove noise and resampled to AVIRIS wavelengths. Endmember groups were then formed by extracting the "tied" spectra in the SWIR2 (2080–2280 nm). The "tying" of spectra, or subtracting the reflectance at the first band from all bands, is performed to eliminate major albedo differences between otherwise similar spectra. The SWIR2 endmembers are then used to calculate the fractional abundance of each endmember in a pixel according to the SMA equations:

$$\rho_{\text{pixel}} = \Sigma[C_e \cdot \rho_e] + \varepsilon = [C_{\text{veg}} \cdot \rho_{\text{veg}} + C_{\text{soil}} \cdot \rho_{\text{soil}} + C_{\text{litter}} \cdot \rho_{\text{litter}}] + \varepsilon \quad (1)$$

$$\Sigma C_e = 1.0, \quad (2)$$

where ρ and C are the reflectance and cover fraction of each endmember, respectively, and ε is an error term. Equation (2) constrains the sum of fractions to equal 1. The unmixing is performed many times on each pixel (~50), each time with endmembers randomly selected from their respective endmember classes. This Monte Carlo method results in a normal distribution of fractions for each pixel, with a calculated mean and standard deviation.

The success of AutoSWIR depends on (1) low variability

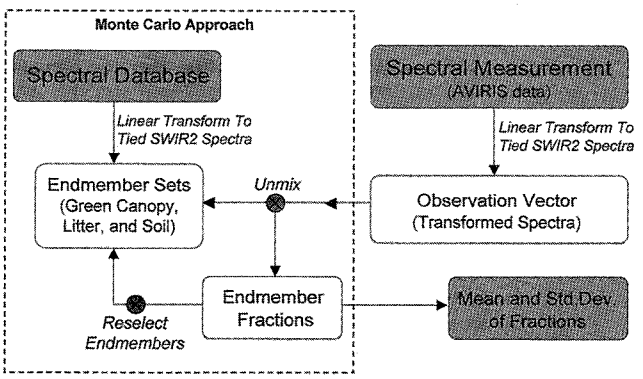

Figure 2. Schematic diagram of AutoSWIR algorithm.

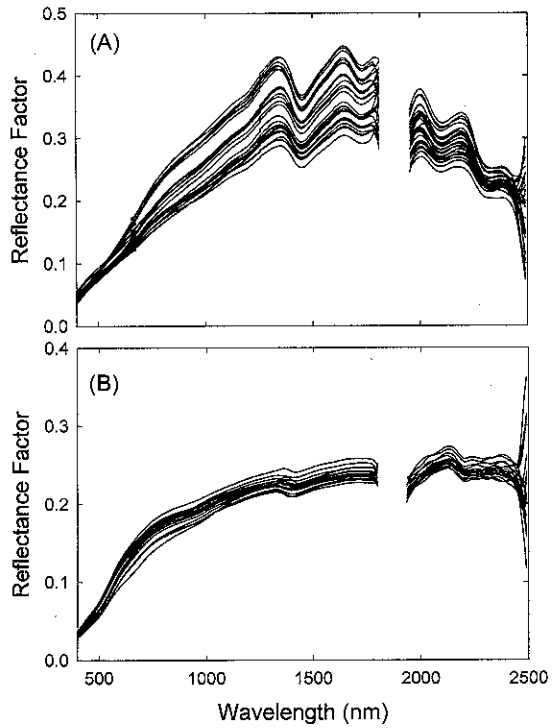

Figure 3. Field spectra of (a) litter and (b) soil from Oregon used in AutoSWIR. Each spectrum shown is the average of 100 individual spectra.

within endmember classes (the tied SWIR2 values), which propagates into a low uncertainty in the derived fractions, and (2) the lack of significant multiple scattering between endmembers in the chosen wavelength region. Low variability in green vegetation endmembers is due largely to strong foliar water absorption features [*Gates et al.*, 1965] (see Figure 1). This minimizes sensitivity to canopy structural properties, such as leaf area index (LAI), since the foliar water absorptions at SWIR2 wavelengths saturate at very low LAI values (~LAI = 1) [*Asner*, 1998]. Low variability in the SWIR2 spectral shape of litter is due to strong absorption features of lignin and cellulose, which are common to all species and produce a strong drop in reflectance beginning at ~2200 nm [*Curran*, 1989]. Finally, SWIR2 spectra of soils are distinguished by clay lattice hydroxyl absorptions near 2200 nm, which are consistent for soils with similar mineralogical and physical properties [*Irons et al.*, 1989].

The diagnostic spectral shapes of each land cover type are exploited by using tied spectra, which remove differences in overall albedo while preserving the linear relation in (1). For example, subtracting the reflectance at one wavelength (ρ_0) is valid, because a spectrum can still be expressed as the properly weighted sum of endmembers:

$$\rho - \rho_0 = C_{veg} \cdot \rho_{veg} + C_{soil} \cdot \rho_{soil} + C_{litter} \cdot \rho_{litter} - (C_{veg} \cdot \rho_{veg,0} + C_{soil} \cdot \rho_{soil,0} + C_{litter} \cdot \rho_{litter,0}) = C_{veg} \cdot (\rho_{veg} - \rho_{veg,0}) + C_{soil} \cdot (\rho_{soil} - \rho_{soil,0}) + C_{litter} \cdot (\rho_{litter} - \rho_{litter,0}). \quad (3)$$

However, a nonlinear spectral transformation, such as dividing by ρ_0, cannot be done within the SMA framework:

$$\frac{\rho}{\rho_0} = \frac{C_{veg} \cdot \rho_{veg} + C_{soil} \cdot \rho_{soil} + C_{litter} \cdot \rho_{litter}}{C_{veg} \cdot \rho_{veg,0} + C_{soil} \cdot \rho_{soil,0} + C_{litter} \cdot \rho_{litter,0}} \neq C_{veg} \frac{\rho_{veg}}{\rho_{veg,0}} + C_{soil} \frac{\rho_{soilg}}{\rho_{soilg,0}} + C_{litter} \frac{\rho_{litter}}{\rho_{litterg,0}}. \quad (4)$$

The Monte Carlo approach is used to quantify the uncertainty in cover fractions caused by any remaining endmember variability. Note that unlike many traditional unmixing approaches, AutoSWIR does not include a shade endmember. Instead, canopy shade is implicitly accounted for within the variability of the green canopy spectral database. In practice, we find that the effect of both canopy and topographic shade is largely removed with the use of tied spectra (see section 3).

It is possible to decrease the number of bands sampled by strategically selecting only a few channels in the SWIR2 region which distinguish between the endmembers. For example, *Asner and Lobell* [2000] used the average reflectance at 2080, 2210, and 2270 nm for each endmember class to form a fixed endmember matrix. Inversion of this matrix led to three simple equations, or indices, used to quickly estimate the fraction of each endmember. Here we test this approach for the 1999 Oregon AVIRIS data using bands 182 (2091 nm), 194 (2210 nm), and 201 (2280 nm). For comparison the normalized difference vegetation index (NDVI) was also calculated:

$$NDVI = (\rho_{810nm} - \rho_{680nm})/(\rho_{810nm} + \rho_{680nm}). \quad (5)$$

The NDVI is extensively used as a metric related to LAI and the fraction of absorbed photosynthetically active radiation (fAPAR) [e.g., *Asrar et al.*, 1984; *Tucker and Sellers*, 1986; *Sellers*, 1987; *Law and Waring*, 1994; *Myneni and Williams*, 1994]. However, NDVI is also affected by several other factors,

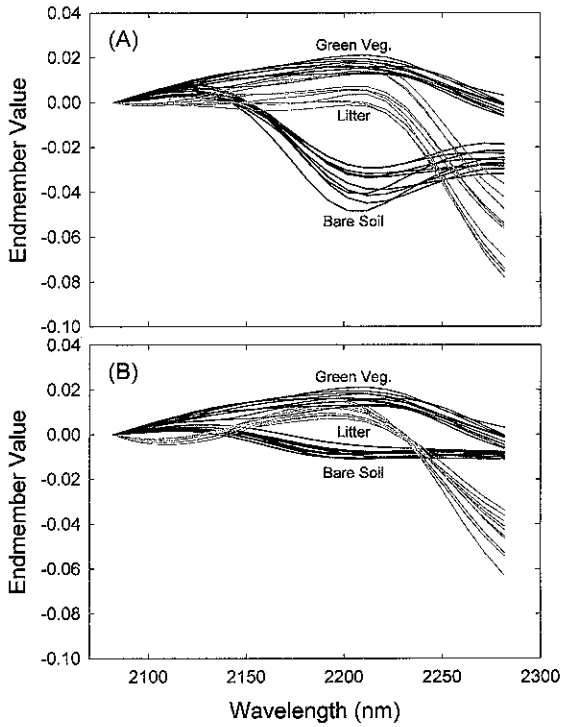

Figure 4. Sample endmember spectra used in AutoSWIR, showing full range of variability for (a) arid endmembers and (b) Oregon endmembers.

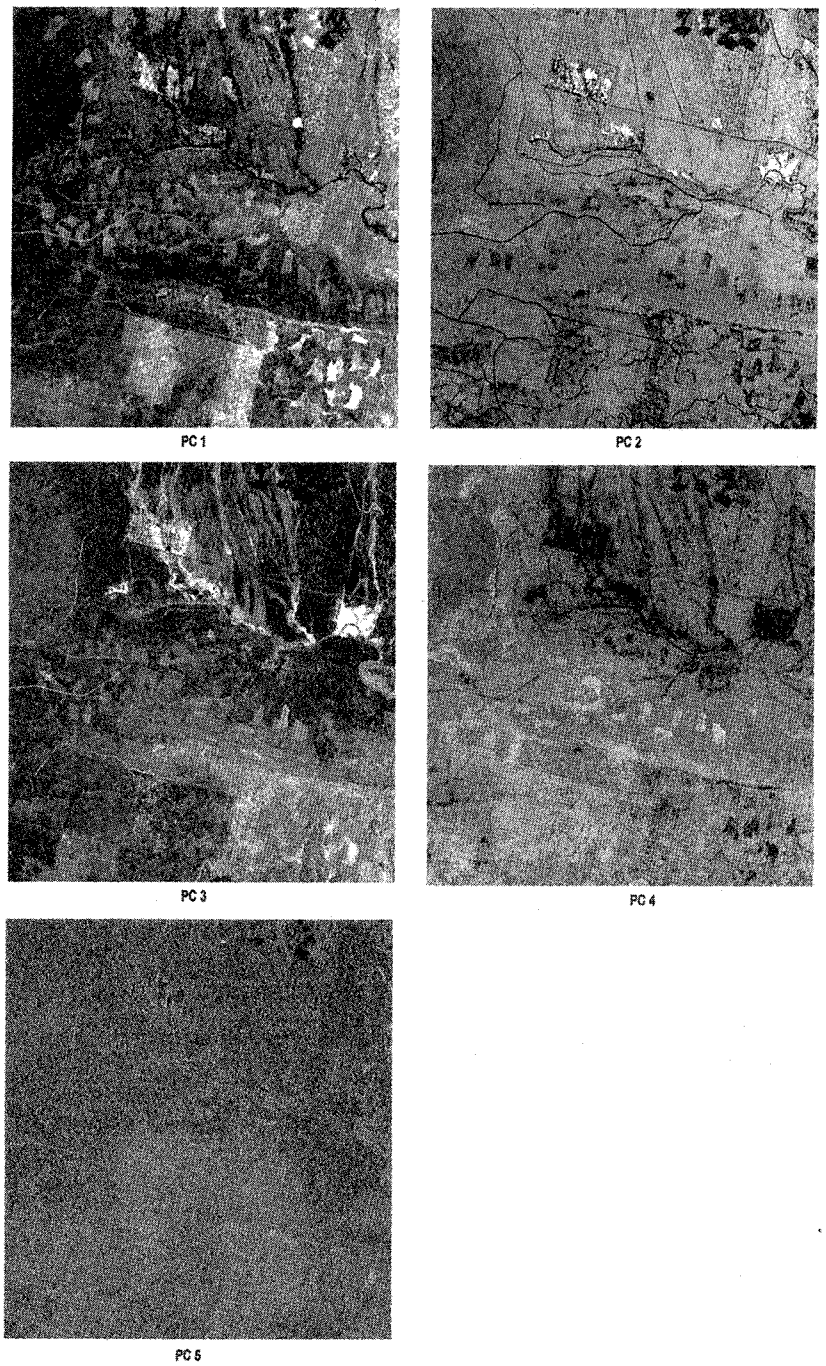

Figure 5. First five principal component images from principal components analysis of SWIR2 bands in AVIRIS subscene, showing the low dimensionality of SWIR2 data.

such as soil and litter reflectance variability and fractional vegetation cover, and therefore at best provides a metric of a pixel's overall "greenness" [e.g., *Huete*, 1988; *van Leeuwen and Huete*, 1996; *Carlson and Ripley*, 1997]. SWIR2 indices developed here have the simplicity of the NDVI while offering the potential to isolate a single physical property of vegetation: the percent cover.

2.4. Air Photo Analysis

Actual vegetation cover was determined at 16 plots using low-altitude air photos from 1997, which were colocated with the AVIRIS imagery in a geographic information system (GIS) using roads and other human-made objects for tie points. The high spatial resolution of the air photos (~2 m) allowed each pixel to be treated as a pure cover type, with ~2500 pixels falling within each plot, and a supervised classification was used to determine the percent vegetation cover (Table 1). Air photos were not available for plots 9, 13, 18, and 20, leaving 16 total plots for analysis.

2.5. Field Spectrometry

To evaluate AutoSWIR with regional endmembers, a field analysis was conducted to measure the optical properties of the soil and litter in the Oregon study region. The data were

collected using a full-range (350–2500 nm) spectrometer with an 18° sensor foreoptic (Analytical Spectral Devices, Inc., Boulder, Colorado). The fiber-optic sensor was positioned <1 m above the soil or litter surface in the nadir position. This instrument collects data in 1.4 nm intervals from 350 to 1100 nm and 2.2 nm intervals in the remaining shortwave-infrared (1100–2500 nm). Measurements were taken within 1.5 hours of solar noon on June 10, 1999, which was a clear day coinciding with the AVIRIS overflight. A total of 30 litter and 17 soil spectra (each an average of 100 individual spectra) were used in this analysis. Because of the height of the major tree species in the study region, canopy-level spectra of green vegetation were not directly measured. Instead, green vegetation spectra from arid lands were used in AutoSWIR along with the Oregon litter and soil spectra. Comparing image spectra from highly vegetated pixels to the arid spectra, which showed similar SWIR2 foliar water absorption features, checked the validity of this substitution (spectra not shown).

2.6. Principal Component Analysis

In the absence of green canopy spectra the consistency of SWIR2 endmember spectra across the scale of the image was investigated using a principal component analysis (PCA). PCA determines the major orthogonal axes of variation that most efficiently describe a given data set and thereby reveals the number of independent axes, or the inherent dimensionality, of the data. In this case, PCA was performed on the SWIR2 spectra (2080–2280 nm) from a 614 × 512 AVIRIS subscene. The dimensionality of the data was determined as the number of bands containing significant spatial information, since variation due to noise is not spatially coherent [*Green et al.*, 1988]. If vegetation canopies of different optical and/or structural properties exhibit a variety of SWIR2 signatures, then we expect a relatively high dimensionality due to variations in these properties across the scene. On the other hand, if all endmembers, including green canopies, have consistent SWIR2 spectral shapes (derivative spectra) and vary mainly in albedo, we expect only three principal components to explain virtually all of the variance in SWIR2 reflectance; that is, one principal component to account for overall brightness, and two for the space of endmember variance (constraining n endmembers to sum to unity results in $n - 1$ independent directions of variance).

3. Results and Discussion

3.1. Field Spectrometry and PCA

The field spectra of litter and soils spanned a wide range of albedos and visible to near-infrared spectral shapes (Figure 3). However, subtracting albedo differences in the SWIR2 greatly reduced the observed variability. The endmembers resulting from the Oregon field survey were compared to the arid endmember sets of *Asner and Lobell* [2000] (Figure 4). The SWIR2-tied spectra for litter in Oregon were very similar to the original arid litter spectra, showing only slightly weaker absorption due to organic compounds [*Curran*, 1989]. Soil spectra, however, were found to have significantly smaller hydroxyl absorptions than were observed in the arid land spectra. This is not surprising because temperate soils contain more organic matter and/or water than arid soils, both of which dampen this absorption feature [*Ben-Dor et al.*, 1999]. The soils at the *P. ponderosa* and *C. decurrens* plots, for example, are sandy loam with ~6% clay. Nonetheless, the soil and litter in Oregon were both found to have spectrally consistent derivatives in the SWIR2, the essential feature for successful application of AutoSWIR.

The results of the PCA helped to demonstrate the consistency of the SWIR2 endmembers at the scale of an AVIRIS image. Figure 5 shows the first five principal component images for an AVIRIS subscene from the analysis. The first three components explained greater than 99.9% of the variance, verifying the prediction that there are three principal directions of variance in the SWIR2. The first eigenvector was primarily responsive to overall brightness in the SWIR2, which is the feature removed by tying spectra in AutoSWIR (Figure 6). The next two eigenvectors represented the remaining dimensionality due to green canopies, senescent vegetation (litter), and soils. Spatial information in the fourth principal component was confined mainly to a golf course located in the region, where the atmospheric correction algorithm ATREM

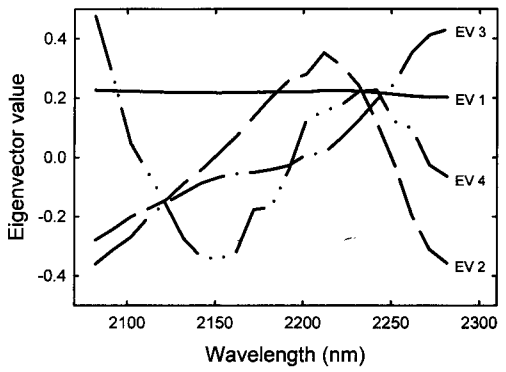

Figure 6. First four eigenvectors from principal components analysis of SWIR2 bands in AVIRIS subscene.

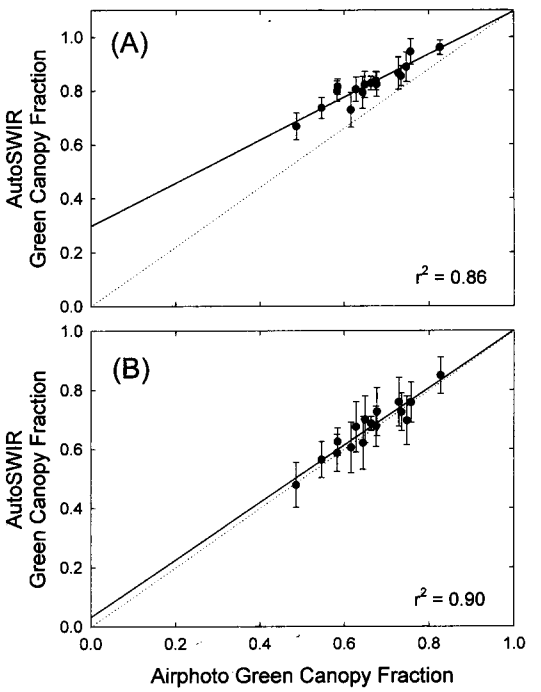

Figure 7. Estimates of green canopy fraction from AutoSWIR with (a) arid endmembers and (b) Oregon endmembers, compared to cover estimates from air photos; 1:1 line (dotted) and best fit line from linear regression (solid) are shown.

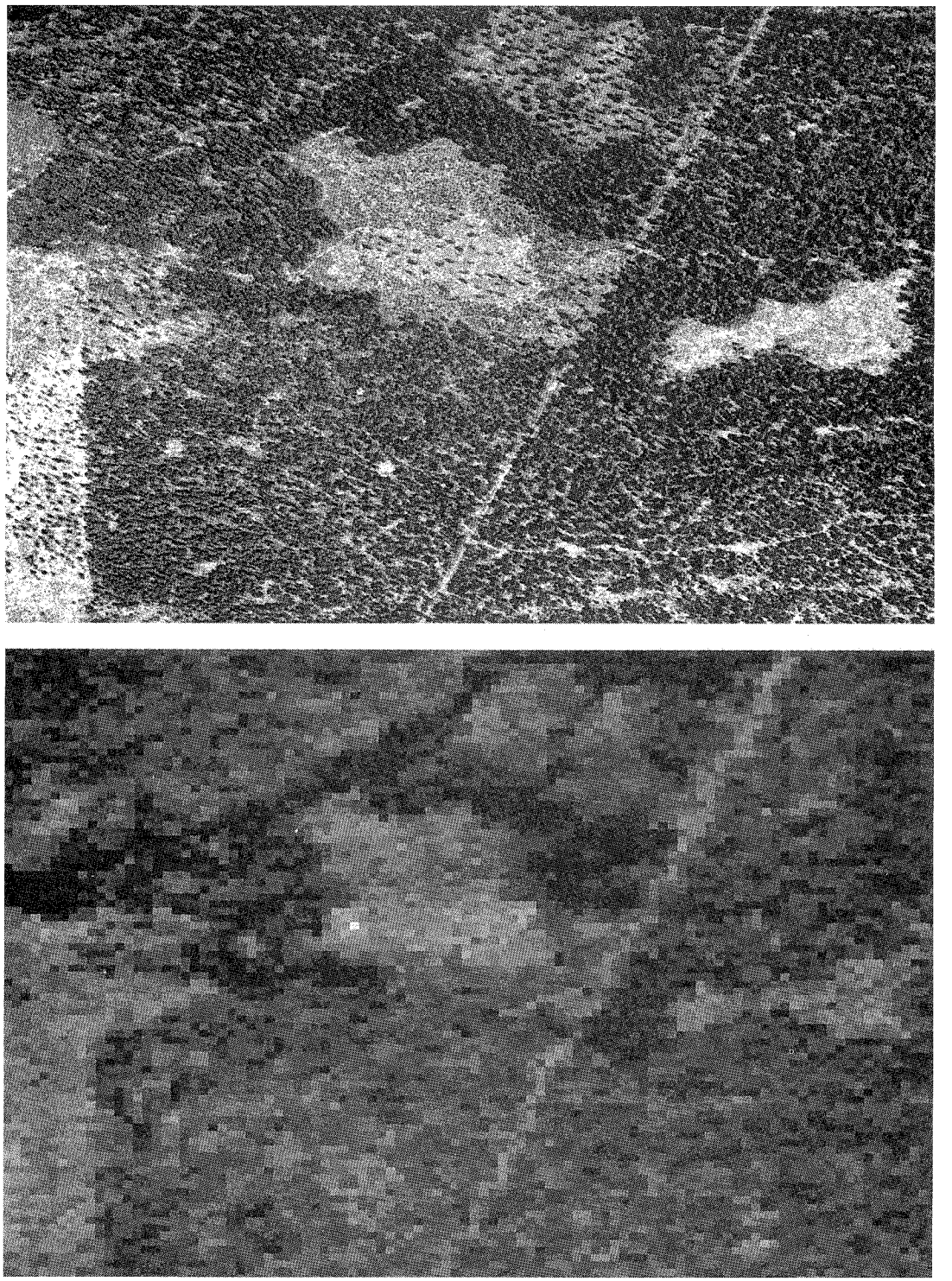

Figure 8. Comparison of air photo (top) and green canopy fractions from AutoSWIR (bottom) for part of study region. Dark pixels in both images signify high vegetation cover.

[*Gao et al.*, 1993] was probably affected by the unnaturally strong foliar water absorptions. Indeed, inspection of eigenvector 4 revealed that it was extremely similar to the transmission spectra of atmospheric water vapor in this wavelength region (Figure 6). All remaining principal components exhibited virtually no spatial information, as demonstrated by principal component 5.

3.2. AutoSWIR

Green canopy fractions calculated by AutoSWIR using the arid land endmembers were consistently higher than air photo estimates (Figure 7a). As expected, the dark organic soils in Oregon were seen as some combination of arid (nonorganic) soil and vegetation when using arid endmembers (Figure 3),

Table 2. SWIR2 Indices and Correlation Statistics With the Full Hyperspectral AutoSWIR Results at Field Plots

Cover Type	Equation	Slope	Offset	R^2
Green canopy	$SWIRVI = 37.72(\rho_{2210} - \rho_{2090}) + 26.27(\rho_{2280} - \rho_{2090}) + 0.57$	0.9489	−0.0037	0.9096
litter	$SWIRLI = 3.87(\rho_{2210} - \rho_{2090}) - 27.51(\rho_{2280} - \rho_{2090}) - 0.20$	1.0571	0.0779	0.9924
soil	$SWIRSI = -41.59(\rho_{2210} - \rho_{2090}) + 1.24(\rho_{2280} - \rho_{2090}) + 0.64$	1.1366	−0.0793	0.9326

resulting in an overestimation of the green canopy fraction. As the true vegetation cover decreased, and the extent of visible bare soil increased, we expected a larger error in vegetation estimates. This trend was indicated in Figure 7a. However, even at ~50% vegetation cover, the error in fraction estimation was only 15%. Thus applying AutoSWIR with arid endmembers resulted in fractions that were spatially realistic but would require rescaling to match field values in regions with relatively low cover.

Substituting the field spectra from Oregon into AutoSWIR greatly improved the green canopy fraction estimates (rms = 3%, Figure 7b). While the relative fit of the best fit line did not greatly improve, the main effect of using Oregon endmembers was to increase its slope to 0.97 and decrease its intercept to 0.03. Therefore in using a relatively small amount of field spectra, we were able to accurately estimate the cover of vegetation without the need for extensive ground-based corrections. Figure 8 illustrates the agreement between the air photo (red band) and vegetation fraction image for part of the study region. Darker pixels represent those with higher vegetation fractions for visual comparison with the air photo, where vegetation was dark and bare soil was bright. The spatial distribution of vegetation in the air photo was similarly well represented in the fraction image throughout the entire study region.

In addition to constraining endmember variability, employing tied SWIR2 spectra has several properties that ultimately distinguish AutoSWIR from traditional methods. First, SWIR2 wavelengths are not adversely affected by multiple scattering, since vegetation is so dark in this region. This contrasts with traditional unmixing methods that use near-infrared wavelengths, where vegetation is bright and multiple scattering leads to nonlinear mixing [*Roberts et al.*, 1993], as well as high endmember variability. In addition, the use of long wavelengths avoids sensitivity to errors in atmospheric scattering corrections, which can influence reflectance at shorter wavelengths [*Vermote et al.*, 1996]. The use of tied spectra also minimizes sensitivity to shading, since the main effect of shade is to lower the overall albedo of a cover's apparent reflectance and not to significantly change the spectral shape (derivative). While shade does slightly dampen the features apparent in tied spectra (e.g., the spectral shape), the variability due to shading conditions is generally within the variability contained in the endmember sets [*Asner*, 1998]. Therefore we contend that utilizing SWIR2 wavelengths has several characteristics that increase the accuracy of cover fraction estimations.

Conversely, potential drawbacks of using SWIR2 measurements include the relatively low signal to noise ratio of instruments that obtain measurements in the SWIR2 [*Green et al.*, 1998], and the sensitivity to absorption of atmospheric gases, such as water vapor and methane. However, as sensor instrumentation and models of atmospheric absorption continue to improve [*Green et al.*, 1998], these issues may be of decreasing concern. The most serious caveat to using AutoSWIR suggested by this study is the potential variability of SWIR2 soil reflectance. In regions with several spectrally distinct soil types, the uncertainty in vegetation cover estimates from AutoSWIR could be significantly increased, as evidenced by the errors incurred when using arid soils for Oregon. In this case, the use of spatial databases of soil spectra could potentially be used to properly constrain the unmixing. A strength of the Monte Carlo approach is that variability in soil spectra is propagated to uncertainty in resulting fractions, allowing a quantitative measure of the effect of soil diversity on each cover fraction.

3.3. SWIR2 Indices

A SWIR2 index for each cover type was derived from the mean Oregon endmembers (Table 2). The high correlation between the indices and the full AutoSWIR procedure suggests that a simple three-band index could provide accurate cover estimates from SWIR2 reflectance. A comparison between the SWIR2 vegetation index (SWIRVI) and the NDVI is shown in Figure 9. While NDVI is roughly correlated with vegetation cover, considerable scatter is present due to variable background reflectance (i.e., soil and litter) and differences in the structure of vegetation canopies between plots. The SWIRVI shows stronger agreement with air photo estimates because it is insensitive to changes in background brightness and canopy structure. Moreover, the SWIRVI estimates a

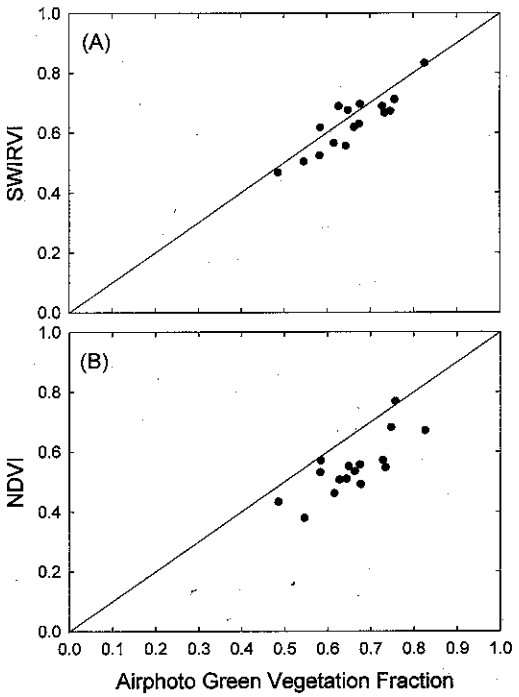

Figure 9. Estimates of green canopy fraction from (a) SWIRVI and (b) NDVI compared to cover estimates from air photos; 1:1 line is shown.

physical quantity (the fractional cover) without the need for empirical fitting or post priori scaling.

4. Conclusions

We have successfully tested an automated SWIR2 spectral unmixing approach for determining canopy cover in a temperate coniferous ecosystem using high spectral resolution remote sensing data. While using field spectra from arid lands led to slight overestimates of vegetation cover, the original algorithm was easily modified with regional field spectra (to represent organic matter presence) to produce highly accurate results. The generality of AutoSWIR allows fast and accurate estimates of vegetation cover that can be used to parameterize physical models and study regional land cover change. By isolating the horizontal extent of vegetation, AutoSWIR also provides a means to deconvolve the often-confused factors of vegetation cover, species, and canopy structure. For example, the estimated cover within each pixel can be used to constrain radiative transfer model inversions for structural properties, such as LAI, using shorter wavelengths [e.g., *Asner et al.*, 1999; *Gilabert et al.*, 2000]. Similarly, isolating the cover of vegetation may provide useful constraints for determining other parameters, such as soil moisture, which are often hindered by the strong effect of vegetation cover [*Clevers*, 1989; *Rao et al.*, 1993].

We see the application of AutoSWIR to estimate cover as an important step toward resolving spatial heterogeneity of vegetated landscapes. The consistency of green vegetation and litter reflectance properties at SWIR2 wavelengths should allow a relatively easy extension of AutoSWIR to new environments, provided that regional soil spectra are available. With SWIR2 reflectance measurements obtained by the forthcoming generation of spaceborne imaging spectrometers, such as the NASA EO-1 Hyperion, the approach presented here has the potential to provide operational estimates of vegetation cover on a global scale. However, investigations of additional ecosystems with diverse soil types are needed to test this claim.

With a more accurate representation of vegetation cover, heterogeneity of landscape properties such as roughness length [*Oleson et al.*, 2000], albedo [*Rowe*, 1993], LAI [*Bonan et al.*, 1993], and soil moisture [*Ghan et al.*, 1997] can be better constrained in atmospheric and hydrological models. This would lead to improved characterizations of processes sensitive to landscape heterogeneity, such as ground heat flux [*Bonan et al.*, 1993; *Yang et al.*, 1999], surface hydrology [*Ghan et al.*, 1997], and carbon exchange [e.g., *Kimball et al.*, 1999]. Such improvements are critical for understanding biophysical and biogeochemical processes and their interactions with land use and climate change.

Acknowledgments. We thank K. Cody and S. Van Tuyl for assistance with the air photo analysis and field data collection, and two anonymous reviewers for their invaluable comments on the manuscript. G. Asner, B. Law, D. Lobell, and R. Treuhaft were supported by NASA OES grant NAG5-8320 (RTOP 622-93-63-40). G. Asner was also supported by NASA New Investigator Program grant NAG5-8709.

References

Asner, G. P., Biophysical and biochemical sources of variability in canopy reflectance, *Remote Sens. Environ.*, *64*, 234–253, 1998.

Asner, G. P., and D. B. Lobell, A biogeophysical approach to automated SWIR unmixing of soils and vegetation, *Remote Sens. Environ.*, *74*, 99–112, 2000.

Asner, G. P., C. A. Wessman, and D. S. Schimel, Heterogeneity of savanna canopy structure and function using imaging spectrometry and inverse modeling, *Ecol. Appl.*, *8*, 1022–1036, 1998.

Asner, G. P., A. R. Townsend, and M. C. Bustamante, Spectrometry of pasture condition and biogeochemistry in the Central Amazon, *Geophys. Res. Lett.*, *26*, 2769–2772, 1999.

Asner, G. P., C. A. Wessman, C. A. Bateson, and J. L. Privette, Impact of tissue, canopy and landscape factors on reflectance variability of arid ecosystems, *Remote Sens. Environ.*, *74*, 69–84, 2000.

Asrar, G., M. Fuchs, E. T. Kanemasu, and M. Yoshida, Estimating absorbed photosynthetic radiation and leaf area index from spectral reflectance in wheat, *Agron. J.*, *76*, 300–306, 1984.

Bateson, C. A., and B. Curtiss, A method for manual endmember selection and spectral unmixing, *Remote Sens. Environ.*, *55*, 229–243, 1996.

Bateson, C. A., G. P. Asner, and C. A. Wessman, Endmember bundles: A new approach to incorporating endmember variability in spectral mixture analysis, *IEEE Trans. Geosci. Remote Sens.*, *38*, 1083–1094, 2000.

Ben-Dor, E., J. R. Irons, and G. F. Epema, Soil reflectance, in *Remote Sensing for the Earth Sciences*, edited by A. N. Rencz, pp. 111–188, John Wiley, New York, 1999.

Bonan, G. B., Land-atmosphere CO_2 exchange simulated by a land surface process model coupled to an atmospheric general circulation model, *J. Geophys. Res.*, *100*, 2817–2831, 1995.

Bonan, G. B., D. Pollard, and S. L. Thompson, Influence of subgrid-scale heterogeneity in leaf-area index, stomatal-resistance, and soil-moisture on grid-scale land-atmosphere interactions, *J. Clim.*, *6*, 1882–1897, 1993.

Carlson, T. N., and D. A. Ripley, On the relation between NDVI, fractional vegetation cover, and leaf area index, *Remote Sens. Environ.*, *62*, 241–255, 1997.

Clark, R. N., Spectroscopy of rocks and minerals, and principles of spectroscopy, in *Remote Sensing for the Earth Sciences*, edited by A. N. Rencz, pp. 3–57, John Wiley, New York, 1999.

Clevers, J. G., The application of a weighted infrared-red vegetation index for estimating leaf area index by correcting for soil moisture, *Remote Sens. Environ.*, *29*, 25–34, 1989.

Cohen, W. B., T. A. Spies, and G. A. Bradshaw, Semivariograms of digital imagery for analysis of conifer canopy structure, *Remote Sens. Environ.*, *34*, 167–178, 1990.

Curran, P. J., Remote sensing of foliar chemistry, *Remote Sens. Environ.*, *30*, 271–278, 1989.

Denslow, J. S., Disturbance and diversity in tropical rain forests: The density effect, *Ecol. Appl.*, *5*, 962–968, 1995.

Gao, B.-C., and A. F. H. Goetz, Column atmospheric water vapor and vegetation liquid water retrievals from airborne imaging spectrometer data, *J. Geophys. Res.*, *95*, 3549–3564, 1990.

Gao, B.-C., K. B. Heidebrecht, and A. F. H. Goetz, Derivation of scaled surface reflectance from AVIRIS data, *Remote Sens. Environ.*, *44*, 165–178, 1993.

Gates, D. M., *Plant-Atmosphere Relationships*, 92 pp., Chapman and Hall, New York, 1993.

Gates, D. M., H. J. Keegan, J. C. Schleter, and V. R. Weidner, Spectral properties of leaves, *Appl. Opt.*, *4*, 11–20, 1965.

Ghan, S. J., J. C. Liljegren, W. J. Shaw, J. H. Hubbe, and J. C. Doran, Influence of subgrid variability on surface hydrology, *J. Clim.*, *10*, 3157–3166, 1997.

Gilabert, M. A., F. J. Garcia-Haro, and J. Melia, A mixture modeling approach to estimate vegetation parameters for heterogeneous canopies in remote sensing, *Remote Sens. Environ.*, *72*, 328–345, 2000.

Green, A. A., M. Berman, P. Switzer, and M. D. Craig, A transformation for ordering multispectral data in terms of image quality with implications for noise removal, *IEEE Trans. Geosci. Remote Sens.*, *26*, 65–74, 1988.

Green, R. O., M. L. Eastwood, and O. Williams, Imaging spectroscopy and the Airborne Visible/Infrared Imaging Spectrometer (AVIRIS), *Remote Sens. Environ.*, *65*, 227–240, 1998.

Hall, F. G., Y. E. Shimabukuro, and K. F. Huemmrich, Remote sensing of forest biophysical structure using mixture decomposition and geometric reflectance models, *Ecol. Appl.*, *5*, 993–1014, 1995.

Houghton, R. A., J. D. Unruh, and P. A. Lefebvre, Current land cover in the tropics and its potential for sequestering carbon, *Global Biogeochem. Cycles*, *7*, 305–320, 1993.

Huete, A. R., A soil-adjusted vegetation index (SAVI), *Remote Sens. Environ.*, *25*, 295–309, 1988.

Irons, J. R., R. A. Weismiller, and G. W. Petersen, Soil reflectance, in *Theory and Applications of Optical Remote Sensing*, edited by G. Asrar, pp. 66–106, John Wiley, New York, 1989.

Jacquemoud, S., F. Baret, and J. F. Hanocq, Modeling spectral and bidirectional soil reflectance, *Remote Sens. Environ.*, *41*, 123–132, 1992.

Kimball, J. S., S. W. Running, and S. S. Saatchi, Sensitivity of boreal forest regional water flux and net primary production simulations to sub-grid-scale land cover complexity, *J. Geophys. Res.*, *104*, 27,789–27,801, 1999.

Law, B. E., and R. H. Waring, Remote sensing of leaf area index and radiation intercepted by understory vegetation, *Ecol. Appl.*, *4*, 272–279, 1994.

Myneni, R. B., and D. L. Williams, On the relationship between fAPAR and NDVI, *Remote Sens. Environ.*, *49*, 200–209, 1994.

Myneni, R. B., J. Ross, and G. Asrar, A review on the theory of photon transport in leaf canopies, *Agric. For. Meteorol.*, *45*, 1–153, 1989.

Oleson, K. W., W. J. Emery, and J. A. Maslanik, Evaluating land surface parameters in the Biosphere-Atmosphere Transfer Scheme using remotely sensed data sets, *J. Geophys. Res.*, *105*, 7275–7293, 2000.

Pielke, R. A., Sr., R. Avissar, M. Raupach, A. J. Dolman, X. Zeng, and S. A. Denning, Interactions between the atmosphere and terrestrial ecosystems: Influence on weather and climate, *Global Change Biol.*, *4*, 461–477, 1998.

Pinty, B., M. M. Verstraete, and N. Gobron, The effect of soil anisotropy on the radiance field emerging from vegetation canopies, *Geophys. Res. Lett.*, *25*, 797–800, 1998.

Price, J. C., How unique are spectral signatures?, *Remote Sens. Environ.*, *49*, 181–186, 1994.

Rao, P. V. N., L. Venkatratnam, and P. V. Krishna, Relation between root zone soil moisture and normalized difference vegetation index of vegetated fields, *Intl. J. Remote Sens.*, *14*, 441–450, 1993.

Roberts, D. A., M. O. Smith, and J. B. Adams, Green vegetation, non-photosynthetic vegetation, and soils in AVIRIS data, *Remote Sens. Environ.*, *44*, 255–269, 1993.

Roberts, D. A., M. Gardner, R. Church, S. Ustin, G. Scheer, and R. O. Green, Mapping chaparral in the Santa Monica Mountains using multiple endmember spectral mixture models, *Remote Sens. Environ.*, *65*, 267–279, 1998.

Ross, J. K., *The Radiation Regime and Architecture of Plant Stands*, Kluwer Acad., Norwell, Mass., 1981.

Rowe, C. M., Incorporating landscape heterogeneity in land surface albedo models, *J. Geophys. Res.*, *98*, 5037–5043, 1993.

Running, S. W., T. R. Loveland, and L. L. Pierce, A vegetation classification logic based on remote sensing for use in general biogeochemical models, *Ambio*, *23*, 77–81, 1994.

Sellers, P. J., Canopy reflectance, photosynthesis, and transpiration, II, the role of biophysics in the linearity of their interdependence, *Intl. J. Remote Sens.*, *6*, 1335–1372, 1987.

Sellers, P. J., et al., Comparison of radiative and physiological effects of doubled atmospheric CO_2 on continental climate, *Science*, *271*, 1402–1406, 1996.

Sellers, P. J., et al., Modeling the exchanges of energy, water and carbon between continents and the atmosphere, *Science*, *275*, 502–509, 1997.

Smith, M. O., J. B. Adams, and D. E. Sabol, Spectral mixture analysis—New strategies for the analysis of multispectral data, in *Imaging Spectrometry—A Tool for Environment Observations*, edited by J. Hill and J. Megier, pp. 125–144, Kluwer Acad., Norwell, Mass., 1994.

Spanner, M. A., L. L. Pierce, D. L. Peterson, and S. W. Running, Remote sensing of temperate coniferous forest leaf area index: The influence of canopy closure, understory vegetation, and background reflectance, *Intl. J. Remote Sens.*, *11*, 95–111, 1990.

Tucker, C. J., and P. J. Sellers, Satellite remote sensing of primary production, *Intl. J. Remote Sens.*, *7*, 1395–1416, 1986.

van Leeuwen, W. J. D., and A. R. Huete, Effects of standing litter on the biophysical interpretation of plant canopies with spectral indices, *Remote Sens. Environ.*, *55*, 123–134, 1996.

Vermote, E. F., et al., Second simulation of the satellite signal in the solar spectrum, 6S: An overview, *IEEE Trans. Geosci. Remote Sens.*, *35*, 675–699, 1996.

Villenueve, P. V., S. A. Gerstl, and G. P. Asner, Estimating nonlinear mixing effects for arid vegetation scenes with MISR channels and observation directions, *Proc. Intl. Geosci. Remote Sens. Symp.*, *3*, 31–35, 1998.

Wessman, C. A., C. A. Bateson, and T. L. Benning, Detecting fire and grazing patterns in tallgrass prairie using spectral mixture analysis, *Ecol. Appl.*, *7*, 493–511, 1997.

Woolley, J. T., Reflectance and transmittance of light by leaves, *Plant Physiol.*, *47*, 656–662, 1971.

Yang, Z.-L., Y. Dai, R. E. Dickinson, and W. J. Shuttleworth, Sensitivity of ground heat flux to vegetation cover fraction and leaf area index, *J. Geophys. Res.*, *104*, 19,505–19,514, 1999.

G. P. Asner and D. B. Lobell, Department of Geological Sciences, Campus Box 399, Benson Earth Sciences Building, University of Colorado, Boulder, CO 80209-0399. (gregory.asner@colorado.edu)

B. E. Law, College of Forestry, Oregon State University, Corvalis, OR 97331.

R. N. Treuhaft, Jet Propulsion Laboratory, California Institute of Technology, Pasadena, CA 91109.

(Received February 11, 2000; revised October 13, 2000;
accepted October 20, 2000.)